Details of the research work duly signed by the applicant, for which the Sun Pharma Research Award is claimed, including references and illustrations (not to exceed 6000 words).

My group has attained a significant place in developing innovative functionalized nano-biomaterials for therapeutic & and diagnostic applications and elucidating the mechanistic aspect of its cellular translocation to achieve a higher therapeutic index with low toxicity of drugs. My focus signify a major role in establishing specific delivery of drugs through innovative nano-therapeutics thereby bypassing the otherwise established biological barriers. My contribution lie basically in two verticals i.e (a) Knowledge generation and development and (b) Translational Contribution and commercialization.
In the segment ***Knowledge generation and development,*** we have explored different mechanisms like *ligand-receptor interactions, endosomal pH responsiveness* and *receptor-mediated endocytosis* and its link to *cancer nano-therapeutics*. This led to high impact publications in the journals of repute. In the other segment ***Translational contribution and commercialization,*** we have successfully developed layer-by-layer (LBL) and SMEDDS technology that impacted product development in the area of bone-related disorders. We have been instrumental in patenting 25 technologies, out of which FIVE have been licensed to Industries while TWO are commercialized as **Joint Fresh™** and **Reunion™** [(Granted US patent 8,496,964; AU Patent; 2010217238A; EP patent 2400957 B1) Other products for the treatment of osteoarthritis and bone loss are also developed (Granted US Patent 10,596,115; AU Patent 2014291615; US patent 10265297)]. In addition, he has been actively involved in developing Umifenovir and its formulation under repurposing for COVID patients whose Phase III clinical trial has been completed.

[A] KNOWLEDGE GENERATION AND DEVELOPMENT: The focus of our research involves engineering biomaterials to explore niche areas of translational research and establish specific delivery of drugs through innovative nano-therapeutics thereby bypassing the otherwise established biological barriers. The development of multifunctional nanoparticles for synchronized imaging and tumor-targeted non-invasive therapy through optical imaging is supposed to have a notable impact on future personalized oncology. These emerging optical fluorescence imaging modality is safe, inexpensive, accurate, and detect cancer at a primitive stage long before the phenotypic changes occur with excellent spatial resolution. In this segment, we have established the role of ***comprehensive nano-theranostics*** with detailed mechanistic understanding that play a pivotal role in rationalizing therapeutic strategy for cancer. We have elucidated Aggregation Induced Emission mechanism demonstrating image-guided chemotherapy through anisamide and Mn+2 functionalized inverse hexagonal particles. He also established proton sponge effect escaping lysosomal degradation by pyridoxine tethered nanoparticles facilitating intracellular localization while modulation of tumor microenvironment using endogenous stimuli-responsive lyotropic nano-liquid crystals ensuing patient-friendly comprehensive cancer nano-theranostics. The detailed strategies discussed in the current context are as follows.

[a] Synchronized Ratio-metric Co-delivery of Metformin and Topotecan through Engineered Mesoporous Silica Nanoparticle Facilitates *in Vivo* Synergistic Precision Levels at Tumor Site.

Theoretically, the success of combination chemotherapy in cancer majorly depends on the ratios of individual agents at the tumor site. Accounting to the dissimilar pharmacokinetic profiles of individual drugs, meagre penetration, and heterogeneous distribution, the redemption of actual synergistic ratios at the target site confronted issues to realize the ultimate therapeutic effect[4]. Delivery of synergistic drug ratios through nano-carriers provides controlled, temporal, and spatial delivery of multiple cargos, enables drug accumulation in tumor, and releases the drugs at a synchronized rate, thereby, probability of maintenance of intracellular synergistic drug concentrations is possible[5,6]. However, co-encapsulation of multiple drugs with different physicochemical properties in the same nano-carrier and controlling the drug release and to achieve required concentration–time profile at the site of action are always challenging tasks.

To overcome these challenges, we developed a novel hydrophobic ion trapping–assisted loading of **Metformin and Topotecan** using pamoic acid (PA) as *in situ* ion trapping agent. The large surface area of MSNs enables to achieve a high payload of both the drugs and in situ ion trapping offers reasonable hydrophobicity to **Metformin**, whereas, **Topotecan** exhibited protagonist for controlling the release. We describe the co-encapsulation of **Metformin** and **Topotecan** in a lipid bilayer–coated mesoporous silica nanoparticles with an aim to achieve high payload and controlled release profile. To shield the surface silanol groups that are highly lipophilic and known to promote nonspecific binding and mononuclear phagocytic system (MPS) uptake[7], the MSNs were camouflaged with lipid bilayer to impart unique attributes which combine the advantages of liposomes with MSNs

A ratio-metric co-delivery platform was developed bearing metformin, a known metabolic modulator and topotecan, a chemotherapeutic drug, by engineering lipid bilayer–camouflaged mesoporous silica nanoparticles that effectively promote apoptosis via mitochondrial membrane depolarization and cell cycle arrest with extended circulation time and higher tumor localization. We developed a novel hydrophobic ion trapping–assisted loading of Metformin (MET) and Topotecan (TPT) using pamoic acid (PA) through ***In Situ Hydrophobic Ion Pairing (HIP)***. The *in vitro* synergy evaluation between MET and TPT using modeling approach is a major highlight of the study, where the derived ratiometric payload of drugs was delivered and evaluated for enhancement of total efficacy of plain drugs in comparison to the mixture of nanoparticles and co-loaded nanoparticles. To develop remote loading procedure, we used PA-loaded LB-MSNs, (PA) LB-MSNs, composed of SoyaPC/cholesterol/1,2- distearoyl-sn-glycero-3-phosphoethanolamine-polyethylene glycol-2000 (DSPE-PEG 2000) at a molar ratio of 7:2.75:0.25 (**Figure 1**A).

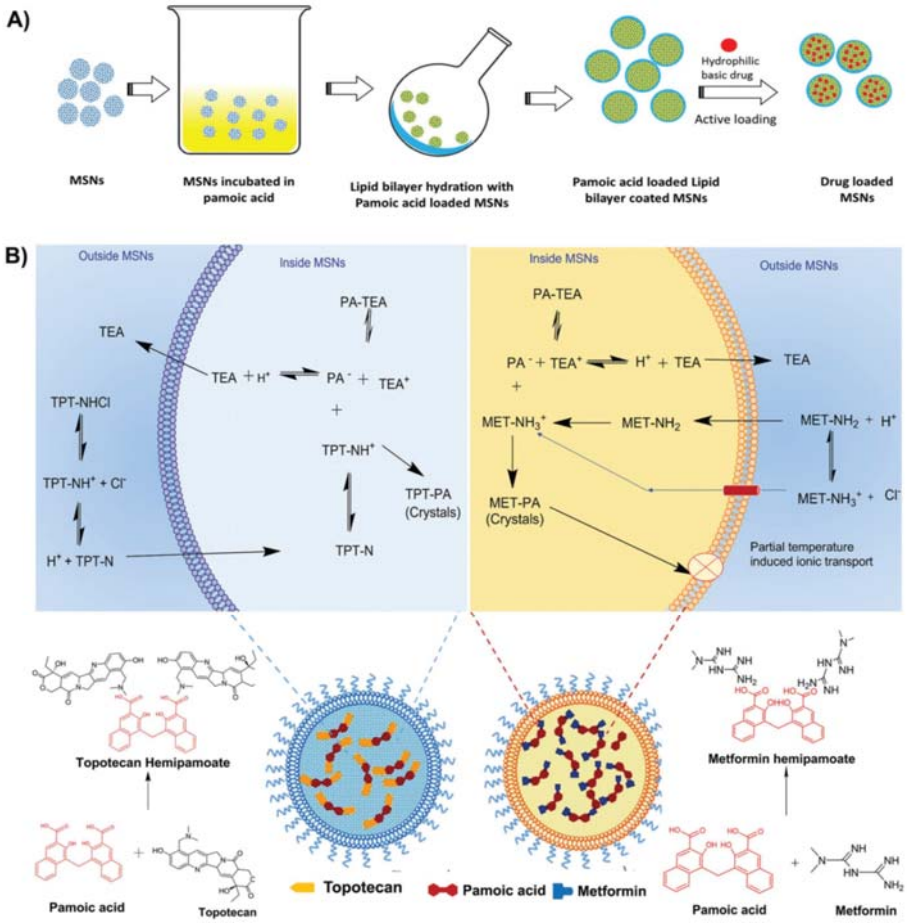

Figure 1. A) Schematics depicting the stepwise preparation of LB-MSNs. B) Mechanistic representation of active loading procedure in PA-loaded LB-MSNs, TEA salt of PA present inside the LB-MSNs allows basic drugs into the MSNs due to gradient difference across the membrane. In case of MET, the higher temperatures partially influence the lipid bilayer permeability. Basic drug after reaching inside MSNs reacts with PA and forms a hydrophobic ion pair (HIP) inside MSN.

Size measurements by DLS technique revealed that the particle size of LB-MSNs was 97.33 ± 5.63 nm, upon loading of PA, the size was slightly increased to 110 ± 8.85 nm (**Figure 2**A). After MTT treatment and obtaining the growth inhibition data, we have used COMBENFIT software package to objectively identify the synergistic combinations of MET and TPT. We assessed the region of the synergy of each combination independently with three established mathematical models, such as Bliss, Loewe, and highest single agent (HSA) models. Based on these modelling data we tried to rationally design the co-loaded LB-MSNs. Initially, we selected six different combinations of MET/TPT. From the MTT assay, it was observed that co-loaded formulations were proven furthermore efficacious compared to a mixture of individual formulations (Figure 3D).

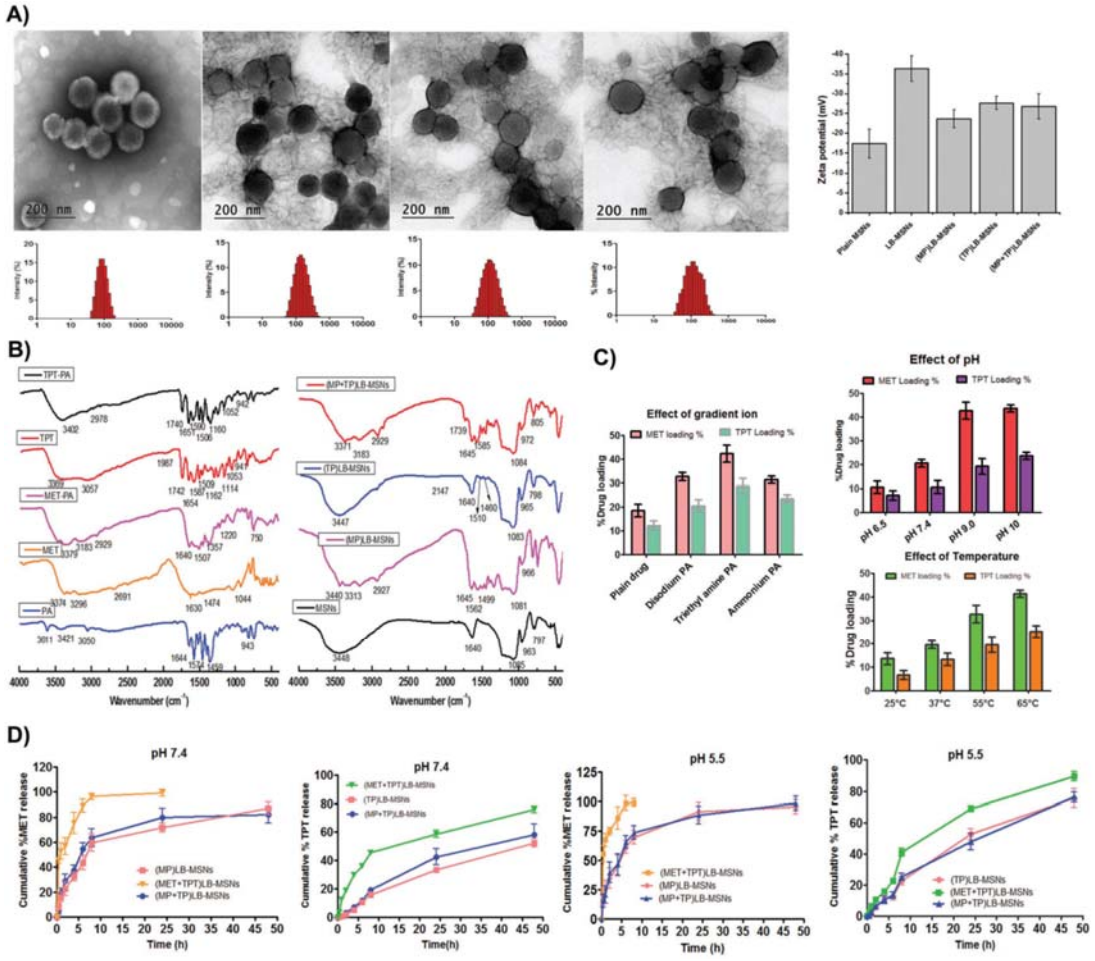

Figure 2. A) Size and polydispersity index (PDI) data of different MSNs, images of transmission electron microscopy (TEM) and dynamic light scattering (DLS) of LB-MSNs, (MP)LB-MSNs, (TP)LB-MSNs, (MP+TP)LB-MSNs (from left to right), and change in zeta potential of different formulations. B) FT-IR of single components (MET, TPT, PA), MET-PA, TPT-PA salts, blank MSNs, and MSNs containing MET, TPT, and PA. C) Various factors affecting the drug loading efficiency; effect of pH, effect of type of gradient ion, and effect of temperature. D) In vitro cumulative percent drug release profiles of MET and TPT from various MSN formulations at pH 7.4 and pH 5.5. All data are expressed as mean } SD (n = 3).

MSNs loaded with MET and TPT, [(MP) LB-MSNs, (TP) LB-MSNs, and (MP+TP)LB-MSNs)] further enhanced the apoptotic effects via mitochondrial membrane depolarization in a synergistic manner. Quantitatively, free MET and TPT induced mitochondrial depolarization in 14.03% and 15.01% cell population, respectively. But, in combination treatment with free drugs slightly enhanced population was observed to be antagonistic. Drug-loaded LB-MSNs significantly enhanced the depolarization representing 27.08% and 31.03% of cell population for (MP) LB-MSNs and (TP) LB-MSNs, respectively. In combination treatment, co-loaded formulation, (MP+TP) LB-MSNs had shown higher depolarization (54.98%) compared to mixture LB-MSNs (42.25%) and Free MET+TPT (20.81%).

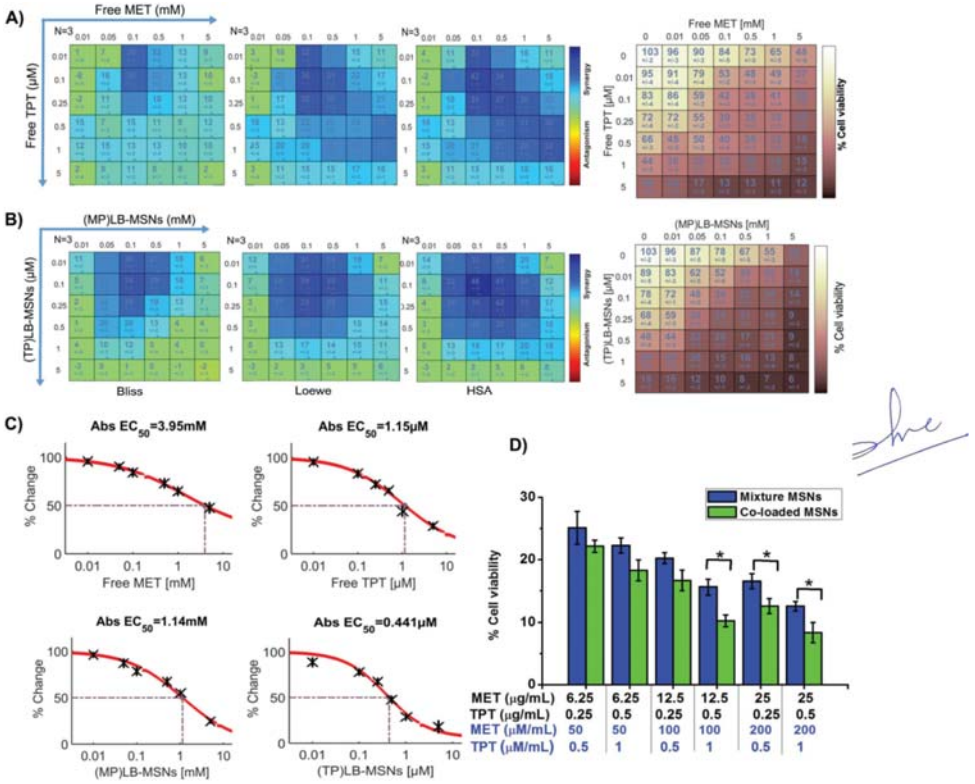

Figure 3. Predicted inhibition data of the three synergy models [Bliss, Loewe, highest single agent (HSA)] in MDA-MB-231 cells treated with A) free MET (*x*-axis) and free TPT (*y*-axis), B) (MP)LB-MSNs and (*x*-axis) and (TP)LB-MSNs (*y*-axis) in 6 × 6 concentration checkerboard format for 48 h using MTT assay. All data are expressed as mean ± SD, $n = 3$, $^{*}p \leq 0.05$; $^{**}p \leq 0.01$; the synergy spots are represented blue in the matrix and experimental data of growth inhibition compared with control are presented. C) Single-agent effect IC50 of the individual drug and drug-loaded LB-MSNs. D) Comparative growth inhibition data of the co-loaded and mixture formulations in definite ratios. All data are expressed as mean ± SD, $n = 3$, $^{*}p \leq 0.05$.

In order to follow the bio-distribution of the LB-MSNs to the tumor site, animals were intravenously injected with near-infrared (NIR)-labeled (DiR740) LB-MSNs, after achieving the 200–300 mm3 tumor size (**Figure 4**A). IVIS imaging was obtained prior to and following IV injection of 1 mg kg−1 equivalent, DiR-labeled LB-MSNs at the designated time points. Robust fluorescence intensity was observed at the tumor sites within 4 h of LB-MSN injection, following which the signal was sustained for at least 24 h. This was also confirmed by *ex vivo* imaging of the tumors and major organs collected from the animals, following sacrifice 24 h post-injection (Figure 4A1,A2). In addition to abundant particle uptake at the tumor site, the liver and spleen were also major sites of particle distribution. Little signalling was obtained in the lung and kidney. The mixture of solutions (MET+TPT solution) and a mixture of single drug loaded MSNs (MP) LB-MSNs+(TP)LB-MSNs had similar effects.

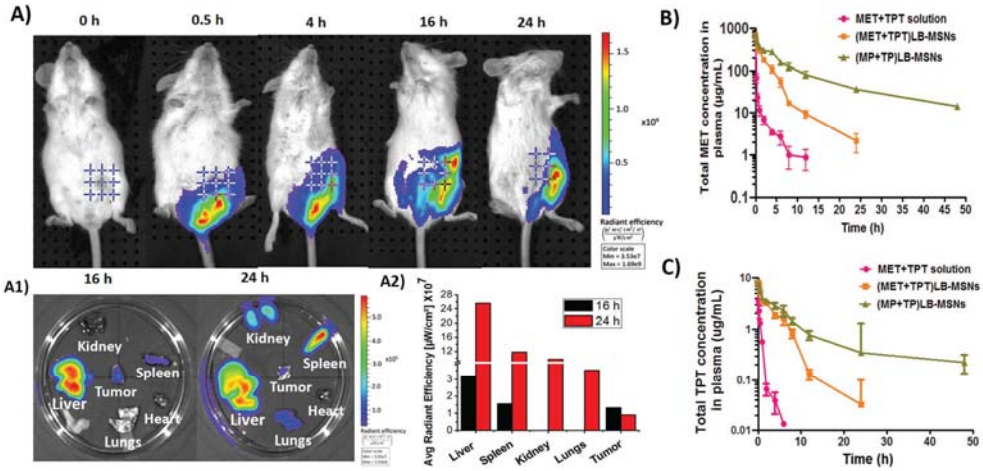

G)

Molar ratio of MET and TPT at the tumor site over 24 h

Time (h)	Molar ratio of MET: TPT at tumor site		
	MET+TPT solution	(MET+TPT)LB-MSNs	(MP+TP)LB-MSNs
0.5	289.51±38.56	386.16±54.23	454.58±53.96
6	40.25±17.30	88.42±14.28	226.88±44.31
24	NA	16.69±4.08	138.91±53.92

Figure 4. A) Representative IVIS images over 24 h to compare the bio-distribution of i.v. injected DiR-labeled LB-MSNs to the 4T1 tumor-bearing mice and A1) ex vivo biodistribution of explanted organs in the same experiment; animals were sacrificed after 16 h and 24 h. A2) Comparative radiant efficiency in different organs of interest. B,C) MET and TPT concentrations in plasma of different coloaded LB-MSNs with and without trapping agent (MET and TPT were given a dose of 50 and 1 mg kg−1, respectively). D) Total MET concentration, E) total TPT concentration in tumor tissue with respect to time, all data are expressed as mean ± SD (n = 3), statistical significance was determined with one-way ANOVA and differences between groups were determined by Tukey's multiple comparison test, *$p \leq 0.05$; **$p \leq 0.01$; ***$p \leq 0.001$; ns, nonsignificant. F) Comparison of total MET and TPT tumor accumulation between the MET+TPT solution and different LB-MSN formulations. G) Molar ratio of MET and TPT at tumor site as free or LB-MSN formulations.

Co-loaded (MP+TP) LB-MSNs showed superior antitumor activity than their solutions and the mixture of single drug loaded LB-MSNs with significant differences ($p \leq 0.05$). The final tumor volume at the end of 20 days post-treatment of co-loaded (MP+TP)LB-MSNs treated group was 13.9-fold, 4.06-fold, and 1.84-fold lower than control, free MET+TPT, and mixture (MP)LB-MSN+(TP) LB-MSN-treated groups, respectively. Whereas, mixture of LB-MSNs had shown 7.5-fold and 2.20-fold lower tumor volumes compared to control and free MET+TPT groups, respectively. The final tumor weight of co-loaded formulation at the end of tumor regression study was 32-fold, 9.69-fold, and 2.29-fold lower than the control group, MET+TPT solution, and mixture(MP)LB-MSN+(TP)LB-MSN group ($p <$ 0.001) (Figure 5B).

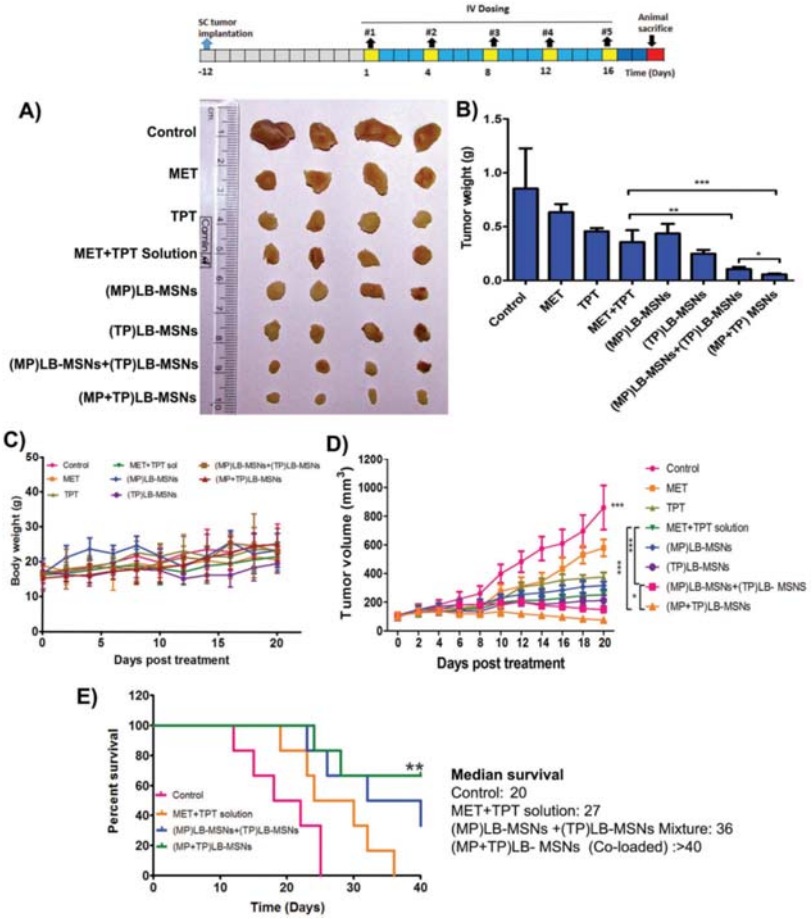

Figure 5. *In vivo* antitumor activity against 4T1 cells transplanted mammary tumor in female BALB/c mice (MET dose: 50 mg kg−1 and TPT dose: 1 mg kg−1 body weight). A) Morphology of the tumors harvested at the end of the study. B) Tumor volume versus time at different time points of the study. All data are expressed as mean ± SD (n = 6), statistical significance was determined with one-way ANOVA analysis. Differences between groups were determined by a Tukey's multiple comparison test, *$p \leq 0.05$; **$p \leq 0.01$; ***$p \leq 0.001$; ns, non-significant. C) Body weight changes during the study period. D) Survival rates of 4T1 tumor-bearing mice administrated with a MET+TPT solution and MET+TPT-loaded LB-MSNs, survival data were generated by the Kaplan–Meier method, median survival and statistical significance were determined by log-rank test and Mann–Whitney U test, respectively (n = 6), **$p \leq 0.01$.

FULL PAPER

Mesoporous Silica Nanoparticles

ADVANCED HEALTHCARE MATERIALS

www.advhealthmat.de

Synchronized Ratiometric Codelivery of Metformin and Topotecan through Engineered Nanocarrier Facilitates In Vivo Synergistic Precision Levels at Tumor Site

*Venkatesh Teja Banala, Shweta Sharma, Puja Barnwal, Sandeep Urandur, Ravi P. Shukla, Naseer Ahmad, Naresh Mittapelly, Gitu Pandey, Monika Dwivedi, Navodayam Kalleti, Kalyan Mitra, Srikanta Kumar Rath, Ritu Trivedi, and Prabhat Ranjan Mishra**

Adv. Healthcare Mater.* 7(19):e1800300 (2018).** ***(Corresponding author)

(I.F. 11.12)

[b] Development and mechanistic elucidation of multimodal nano-theranostic enabling spatial targeting to tumor for imaging and enhanced therapeutic efficacy.

(i) It is the need of hour to have therapeutic strategy with a combination of diagnostic and therapeutic functions into one theranostics systems as an all-in-one approach for better patient compliance. We have elucidated the role of anisamide anchored hexagonal nano-liquid crystals against breast cancer with significantly enhanced efficacy along with non-invasive image-guided chemotherapy through Aggregation Induced Emission (AIE) effect using Tetraphenylethene (TPE) as fluorophores.

We have demonstrated that aggregation-induced emission (AIE) property imparted by Tetraphenylethene (TPE) outperforms the flaws of inorganic contrast agents like small Stokes shift, low photostability, low molar absorptivity and heavy metal cytotoxicity[1]. TPE is a propeller-shaped molecule, which, in the dissolved state, possesses torsional motions capable of relaxing the energy of absorbed photons non-radiatively, whereas on aggregation, they promote efficient photoluminescence due to the restriction of their intra-molecular rotations (RIR). It was used to demonstrate that TPE has advantage over conventional organic dyes, which are highly emissive when dissolved, but once clustered in the nanoparticles, aggregation-caused quenching (ACQ) of fluorescence limits the doping amount of dyes, which cannot be swapped by simply increasing the amount of dye concentration. Besides, the unique property to overcome the ACQ effect of conventional organic fluorophores, safety profile along with high “off−on” contrast ratio, large Stokes-shifted fluorescence, long luminescence lifetime, strong photobleaching resistance, and simple and cheap chemical synthesis of TPE-based materials have driven us to select TPE over other AIEgens[2].

In this area we have developed an inverse hexagonal (HII) phase liquid crystals for the development of multimodal nanoparticles ensemble of tumor-targeting, imaging and therapeutic properties simultaneously. Initially, we have designed a novel sigma receptor ligand, anisamide (AA)-grafted Pluronic F127 (PF127), using carbodiimide chemistry for the stabilization of glyceryl monooleate (GMO)-based nanoparticles (NLC NPs). Further, the AIE effect was imparted using tetraphenylethene (TPE), an iconic fluorogen in combination with a phytoestrogen, formononetin (FMN), for its spatiotemporal release. For this purpose, GMO-based NLC NPs stabilized by PF127/PF127-AA mixture was loaded with the FMN and TPE (AA-NLC-TF). The synthetic scheme and proposed model illustrating the AIE-based active bio-imaging in vitro and in vivo are shown in Scheme 1.

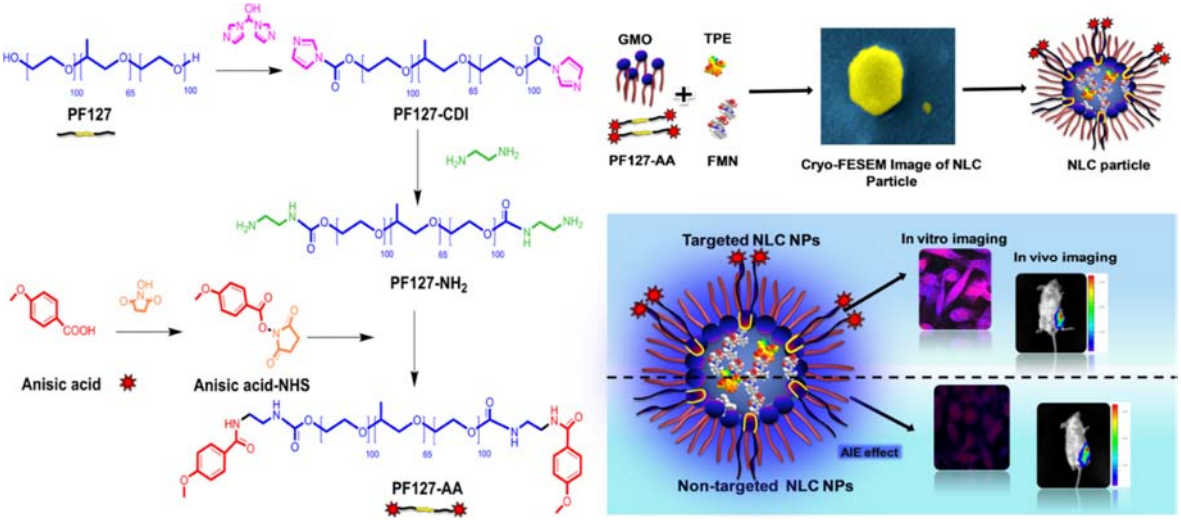

Scheme 1: Schematic Illustration of Synthetic Steps for PF127-AA and Schematic Illustration of AIE-Based Active Bio-imaging in Vitro and in Vivo

The size of the nanoparticles obtained was suitable for accumulation at the tumor site by enhanced permeability and retention effect as observed with Cryo-FESEM, TEM, and AFM images (Figures 2and 3). Structural parameters like lattice parameters and water channel radii for AA-NLC-TF is 61.0 ± 0.2 (Å) and 33.1 ± 0.2 r_w (Å) respectively. Inspection of NLC particles through TEM revealed that the particles possessed hexagonal symmetry. Typically, HII phase liquid crystalline particles consist of water-filled continuous cylindrical lipid matrix arranged in the hexagon shape, and as shown in the TEM photo image (Figure 2A).

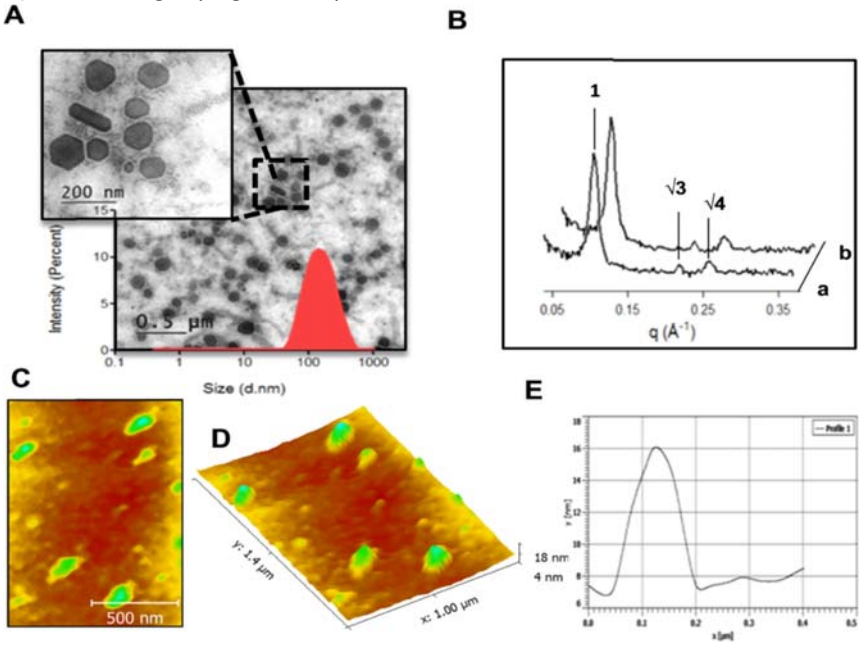

Figure 2: Size and morphological characterization of NLC NPs by (A) TEM (scale bar, 200 nm) and particle size distribution of AA-NLC-TF particles. (B) SAXS intensity plots of (a) blank NLC particles and (b) AA-NLC-TF. AFM images of AA-NLC-TF particles (C) AFM two-dimensional image (scale bar, 500 nm) and (D) 3D view. (E) Height profile.

It was observed that, due to AIE property of TPE trapped in the crystalline core, liquid crystalline particles shows bright blue emission under 365 nm UV light. The presence of AA-NLC-TF nanoparticles in water was also confirmed by shining a laser beam through the nanoparticle solution to observe the Tyndall effect. The absorption and fluorescence emission spectra of AA-NLC-TF were measured. The existence of AIE effect in the nanoparticles was evidenced through the photo-physical studies that advocate the application of NLC NPs in fluorescence-based bio imaging.

Results showed that the apoptotic effect of AA-NLC-TF in MDA-MB 231 cells was more pronounced than free FMN treatment. The apoptotic effect of AA-NLC-TF (33.55%) was higher compared to the apoptotic of NLC-TF (22.88%), free FMN (12.22%), blank NLC (2.56%). As stated previously sigma receptors played a vital role in the uptake of AA-NLC-TF. Reduced apoptotic effects observed after treatment with NLC-TF may be due to its non-targeting property, and findings summarized in the Figure 3A demonstrate the apoptotic effect of treatment regimens and free drug.

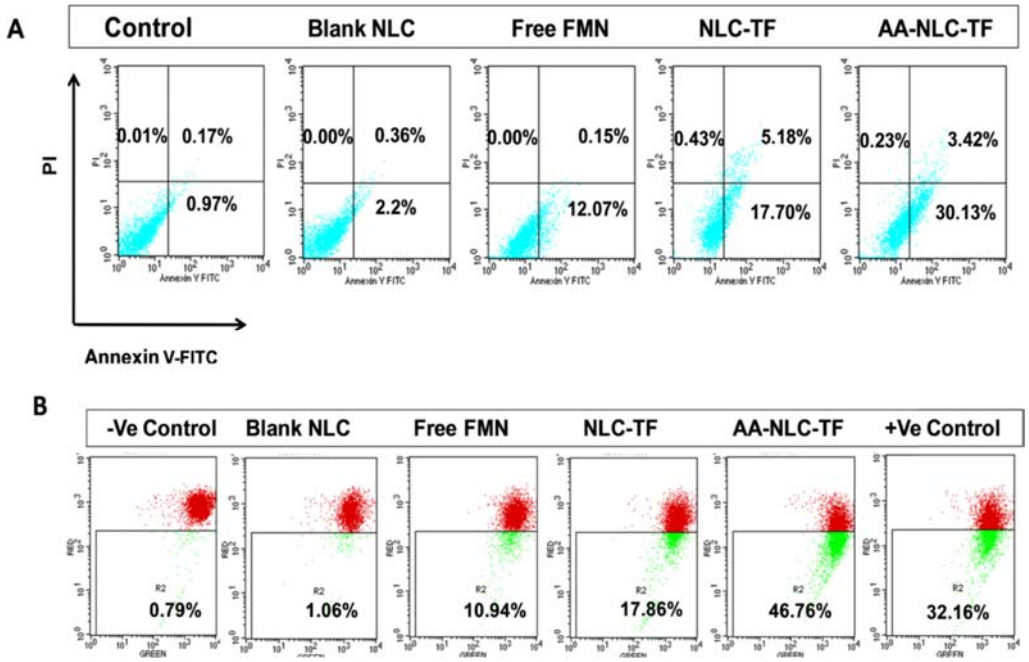

Figure 3: A) Dot plots representing the level of apoptosis in MDA-MB 231 cells after treatment with blank NLC, free FMN, NLC-TF, and AANLC-TF for 48 h. (B) Mitochondrial membrane potential of MDA-MB 231 cells generated after treatment with blank NLC, free FMN, NLC-TF, and AA-NLC-TF for 24 h. PBS-treated cells served as negative control, whereas FCCP-treated cells served as positive control.

Figure 4A, B shows (In vivo imaging) the time dependent tumor accumulation of TPE-loaded nanoparticles in 4T1- cells induced tumor bearing mice when observed using IVIS Kinetic Imaging System. High intense fluorescence was observed after 12 h post-injection of AA-NLCTF when compared to NLC-TF treated group, indicating higher localization of targeted nanoparticles (AA-NLC-TF) in the tumor tissue. The capability

of the TPE loaded AA-NLCTF nanoparticles to illuminate the tumor tissue selectively with high contrast may be associated with intense fluorescence of AIE fluorogen -TPE accumulated in the tumor and active tumor targeting ability of the nanoparticles by the AA ligand.

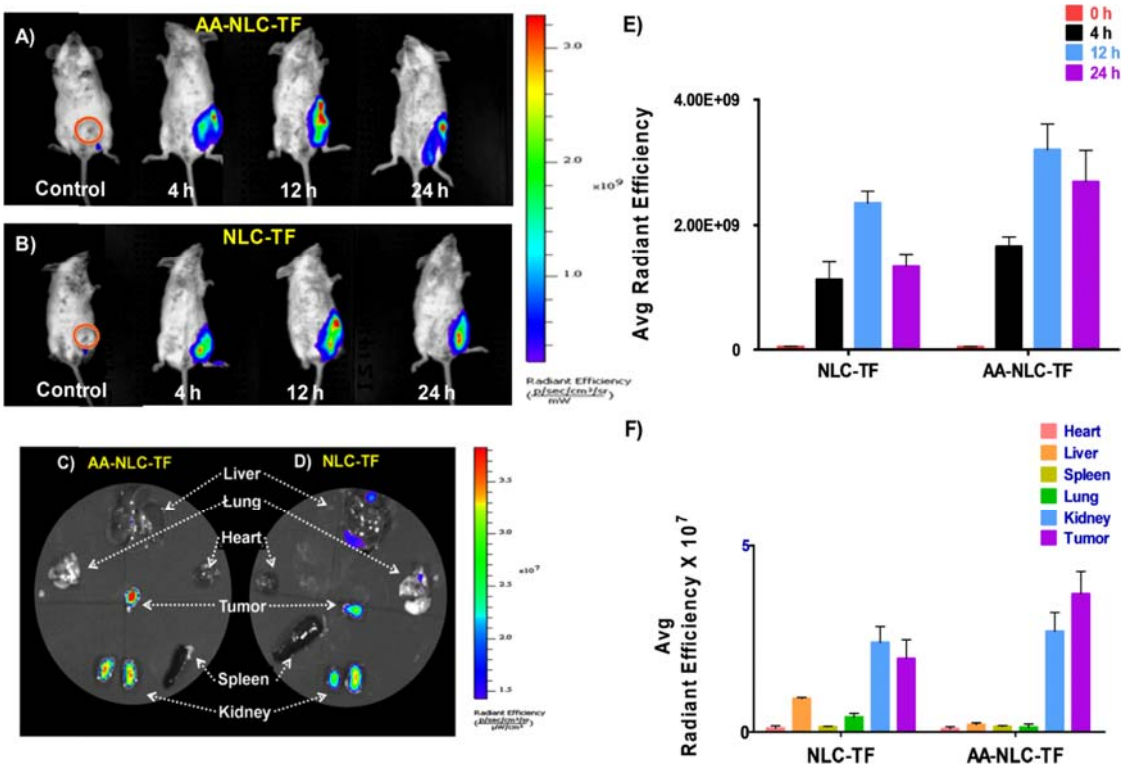

Figure 4: In vivo tumor imaging and tumor-targeting study after iv injection of NLC formulation. (A, B) Body imaging of targeted group and nontargeted group; tumor locations were marked by red circles. (C, D) Ex vivo imaging of major organs from 4T1 tumor-bearing mice at 12 h post injection of the above-mentioned group. (E) In vivo quantification of tumor-associated fluorescence signals of TPE-loaded NLC NPs. (F) Ex vivo quantification of fluorescence signals of TPE-loaded NLC NPs in other major organs. All data are shown as mean ± SD (n = 3).

In vivo antitumor efficacy studies (Figure 5) in 4T1 breast carcinoma transplanted in BALB/c mice (FMN dose: 10 mg/kg body weight) reveals that the average tumor volume of the free FMN treated groups was significantly lower than that of the control group, and the tumor volume of the AA-NLC-TF group was significantly smaller than that of both NLC-TF treated group ($p < 0.001$) and the control group ($p < 0.05$). The results indicated that the active targeting of FMN in NLC-NPs improved its efficacy than free FMN. Compared to control mice, the weight of NLC formulations and free FMN treated mice were remained almost unchanged, these indicate the *in vivo* biocompatibility of the NLC NPs.

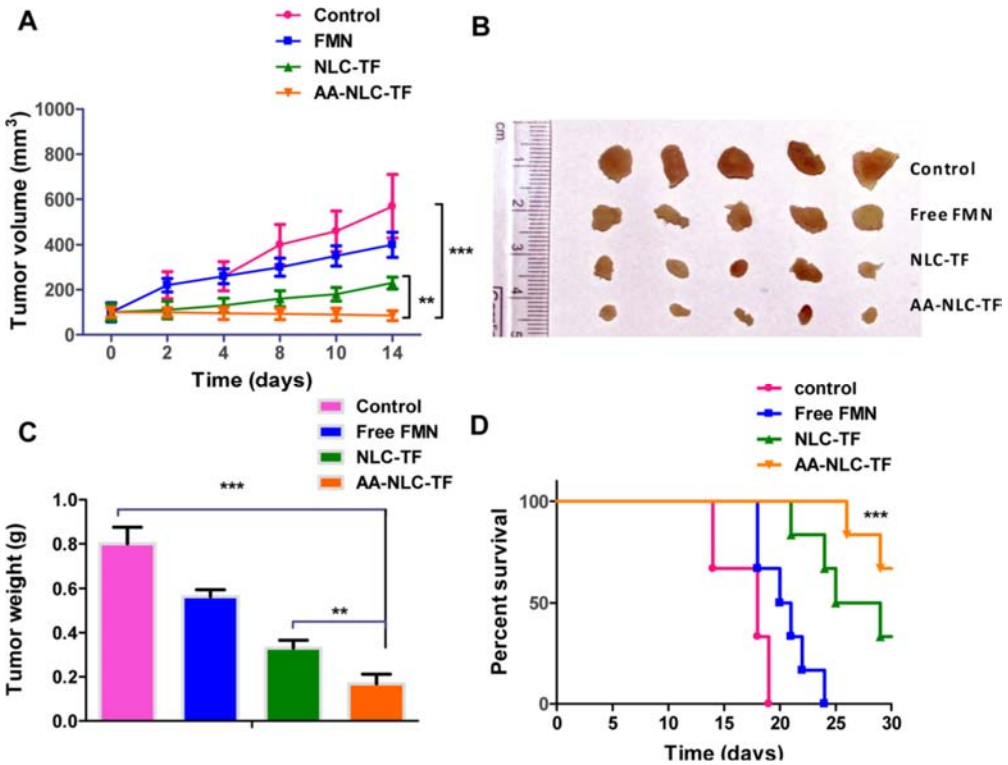

Figure 5: In vivo antitumor activity against 4T1 cells transplanted mammary tumor in BALB/c (FMN dose: 10 mg/kg body weight). (A) Tumor volume vs time at different time points of the study (n = 6). (B) Morphology of the tumors harvested at the end of the study. (C) Weights of the tumors excised at the end of the tumor regression study. (D) Survival rates of 4T1 tumor-bearing mice (n = 6); ***P < 0.001 represents control vs AA-NLC-TF, and **P < 0.05 represents NLC-TF vs AA-NLC-TF.)

Publication:

ACS APPLIED MATERIALS & INTERFACES

Research Article

Cite This: ACS Appl. Mater. Interfaces 2018, 10, 12960−12974

www.acsami.org

Anisamide-Anchored Lyotropic Nano-Liquid Crystalline Particles with AIE Effect: A Smart Optical Beacon for Tumor Imaging and Therapy

Sandeep Urandur,[†] Venkatesh Teja Banala,[†] Ravi Prakash Shukla,[†] Naresh Mittapelly,[†] Gitu Pandey,[†] Navodayam Kalleti,[‡] Kalyan Mitra,[§] Srikanta Kumar Rath,[‡] Ritu Trivedi,[∥] Pratibha Ramarao,[⊥] and Prabhat Ranjan Mishra*[,†]

ACS Appl. Mater. Interfaces, *10(15) 12960-12974 (2018) (Corresponding author);* *IF 10.38*

(ii) Similarly, we also established that, tumor microenvironment can be modulated using **Mn2+ functionalized theranostic lyotropic liquid crystalline nanostructures** (LCNs) as a new theranostic arsenal without any external stimulus to achieve advanced comprehensive cancer nano-theranostics**.** Compared to radiation, photodynamic and photothermal therapy, the selective activation of tumor micro-environmental endogenously for logical generation of cytotoxic OH free radicals serves as an efficient therapeutic strategy for chemodynamic-cancer treatment[3]. MNPs serves as a fluorescent agent as well as a source of manganese (Mn^{2+}) that enables localized oxidative stress under the hallmarks of cancer (acidosis, high H_2O_2 level).

In pursuit of synergistic amplification of Mn^{2+} antitumor activity, Mn-Oleate (MO) complex was synthesized & Fenton catalyst MnO nanoparticles were developed wherein betulinic acid (BA) was loaded in LCN's. In this investigation, nano-architecture of LCN's phase interface is established via SAXS, Cryo-TEM and Cryo-FESEM. Intriguing *in vitro* studies showed that the LCN's triggered hydroxyl radical production and exhibited greater selective cytotoxicity in cancer cells, ensuring safety of normal cells. Significant tumor ablation is realized by 96.5 % of tumor growth inhibition index of LCN's as compared to control group. Key insights into on-site drug release, local anti-cancer response, and tumor location are gained through precise guidance of fluorescent MNPs. In addition, comprehensive assessment of the safety, pharmacokinetics and tumor distribution behavior of LCN's is performed *in vivo* or *ex vivo*. To boost Mn's anti-cancer activity, LCN@Mn-BA was loaded with betulinic acid (2.8×10^{-1} wt%) dependent on the synergistic proportion of Mn and BA obtained from the drug combination experiment. Presence of Mn, O elements was confirmed in the formulation by its unique set of peaks in the electromagnetic emission spectrum (***Urandur et al Acta Biomatarialia 2020***).

Disodium terephthalate (TA) based fluorescence method was used to determine the Fenton-like catalyst activity of LCN@Mn- BA in the presence of H_2O_2, and we explored it by generating OH• radicals under different pH conditions (Fig 1). This work emphasizes the promise of modulating tumor microenvironment with smart endogenous stimuli sensitive nano systems to achieve advanced comprehensive cancer nano-theranostics without any external stimulus. In this investigation, MnO nanoparticles fulfill two needs (fluorescence based optical imaging and a source of Mn^{2+} based chemodynamic therapy) in one unit. This approach also ensures the safety of normal cells, as the toxic OH ·free radical activity is substantially suppressed under the mild alkaline/H_2O_2 conditions in normal cell microenvironment.

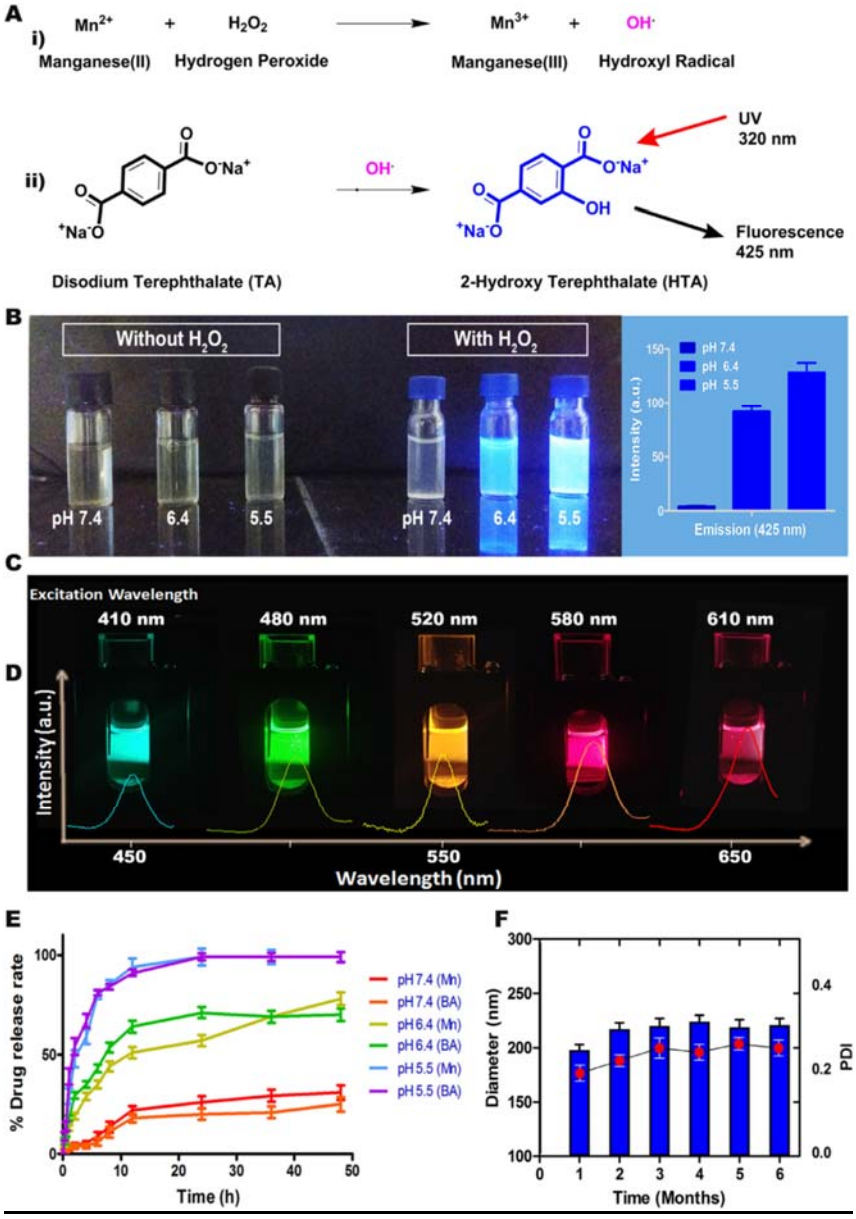

Fig. 1. A) Schematic illustration of i)Fenton like reaction between manganese(II) and hydrogen peroxide generate highly reactive hydroxyl (OH•) radicals that cause oxidative stress in cancer cells. Disodium terephthalate, a sensitive probe for OH• radicals was used to detect and to confirm the production of OH• radicals; (ii)OH• radicals were detected through the formation of fluorescent 2-hydroxy terephthalate on reaction with disodium terephthalate. B)Digital photographs confirms generation of ROS at different pH without or within the presence of H_2O_2 and fluorescence emission spectra of LCN@Mn-BA at different pH in the presence of H_2O_2. C) Images showing fluorescence emissions of MNP nanoparticles dispersion at different excitation wavelengths and D) corresponding fluorescence emission spectra. E) *In vitro* drug release profile of LCN@Mn-BA at various pH conditions at 37 °C for 48h. F) Physical stability studies of LCN@Mn-BA conducted in PBS pH 7.4 at 25 °C for six months. All the (E,F) data are expressed in mean ±S.D, n = 3.

The prominent LCN@Mn-BA tumor deposition was also proved using ex-vivo study of excised tumor tissue and other organs. After 24h, high fluorescence intensity was observed in tumor and liver while minimal signals were received from the other

organ such as lungs that might be due to passive accumulation of nanoparticles (Fig. 2 B and D).

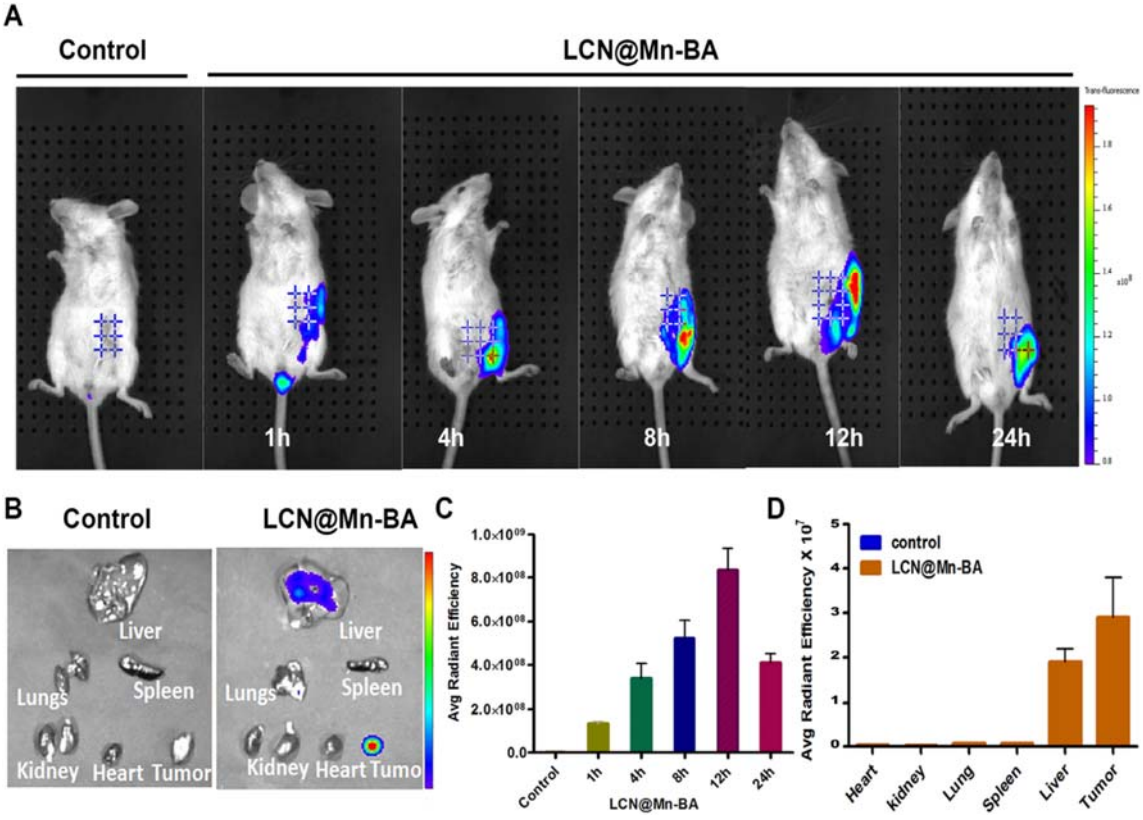

Fig. 2. *In vivo* tumor imaging after i.v. injection of LCN@Mn-BA formulation (1 mg/mL MNP equivalent); A) Body imaging of control and treated group; B) *Ex-vivo* imaging of control and LCN@Mn-BA treated group organs at 24 h of post injection; C, D) *In vivo* quantification of tumor and organs associated fluorescence signals of LCN@Mn-BA nanoparticles.

It was observed that LCN@Mn-BA's anti-tumor efficacy was 6 fold higher than the Mn + BA cocktail and 29 fold higher than control (Fig. 3A). The quantitative tumor growth inhibition index (TIX) rates were 97 ±3 % for LCN@Mn-BA and 75 ±4% for Mn + BA cocktail compared to control. Furthermore, the TIX rate of LCN@Mn-BA was 22±3 times higher than the treatment group for Mn+BA cocktail (Fig. 3B). During this therapeutic period, control group and all therapeutic groups showed no significant variations in body weight indicating no significant toxicity was induced in mice by injection of LCN@Mn-BA, LCN@Mn nanoparticles or free drugs during therapeutic treatment (Fig. 3C). After administration of LCN@Mn-BA nanoparticles, as shown in Fig. 3D mice tumors were dissected and compared to visually demonstrate effective tumor suppression rate. As shown in Fig. 4 E, medial survival time of control, Mn, BA, Mn+BA, LCN@Mn and LCN@Mn-BA was as follows: 25, 27, 32, 40, > 50 days and > 50 days respectively.

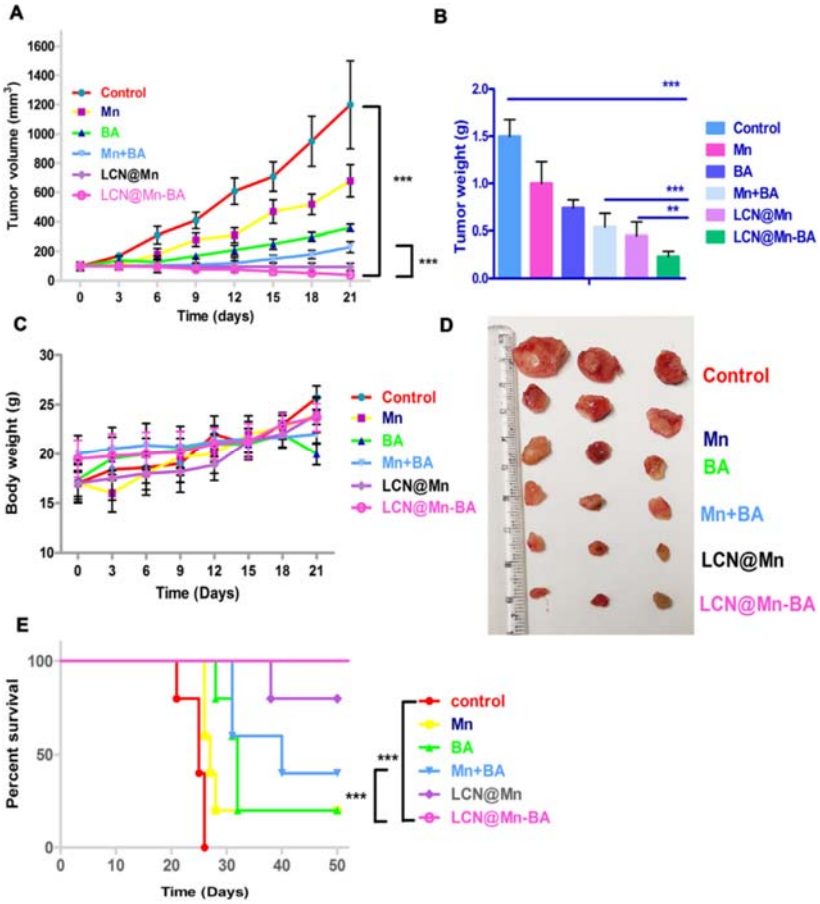

Fig. 3. *In vivo* therapeutic performance of LCN@Mn-BA against 4T1 tumor xenografts. A) tumor volume; B) tumor weight; and C) body weight of 4T1 tumor bearing mice treated with saline (control group), Mn, BA, Mn + BA cocktail, LCN@Mn and LCN@Mn-BA. D) Representative image of tumors dissected at the end of 21 days study. E) The percentage of survival of 4T1 tumor-bearing mice treated with Mn, BA, Mn+BA cocktail, LCN@Mn, LCN@Mn-BA and saline (control group). The data represented as mean ±SD. The free drugs or LCN's formulation equivalent to dose of 10 mg/kg of BA and 40 mg/kg of Mn were used in the study. $*p < 0.05$, $**p < 0.01$, $***p < 0.001$ ($n = 5$ in each treatment group).

Acta Biomaterialia 113 (2020) 522–540

Contents lists available at ScienceDirect

Acta Biomaterialia

journal homepage: www.elsevier.com/locate/actbio

Full length article

Theranostic lyotropic liquid crystalline nanostructures for selective breast cancer imaging and therapy

Sandeep Urandur[a], Venkatesh Teja Banala[a], Ravi Prakash Shukla[a], Shalini Gautam[a], Disha Marwaha[a], Nikhil Rai[a], Madhu Sharma[a], Shweta Sharma[a], Pratibha Ramarao[b], Prabhat Ranjan Mishra[a,*]

[a] Pharmaceutics and Pharmacokinetics Division, CSIR-Central Drug Research Institute Lucknow, Sector-10, Jankipuram Extension, Sitapur Road, Lucknow 226031, India
[b] Soft Condensed Matter Lab, Raman Research Institute, Bangalore, India

113, 522–540 (2020) ***(Corresponding author)*** ***(I.F. 10.63)***

[c] Pyridoxine modified pH Responsive Lipid Nanoparticles not only Trigger Intracellular Delivery of Doxorubicin but also facilitate endosomal escape through proton sponge effect

(i) There are several reports on pH responsive nano-particulate carrier system for intracellular delivery, however triggered release at endosomal pH is not enough for maximum efficacy. This is because nanoparticles usually enter the cells through adsorptive endocytosis (non-specific) or receptor-mediated endocytosis (specific) and if not escaped from endo/lysosome they eventually get degraded or digested by the endosomal enzymes[8]. This degradation often results in limited delivery of drugs to the intracellular targets. Therefore, development of delivery system that can facilitate drug escapement from the endosomal/lysosomal environment is very important [9].

We have established the role of pyridoxine teethered nanoparticles in escaping lysosomal degradation at low pH to achieve fifteen fold reduction in therapeutic dose of doxorubicin with enhanced antitumor efficacy. To achieve this we have developed pH responsive nanoparticles that not only trigger the release of drug at acidic pH, but also facilitate the process of endosomal escape by generation of cationic charge. This cationic charge absorbs the protons of acidic environment by means of specific chemical groups and then causes swelling or rupture of the endo/lysosome. The nanoparticles with charge reversal properties present best approach for systemic administration and tumor targeting because they remain negatively charge at blood pH 7.4, thereby reducing the uptake by RES system, but become positively charged at the tumor site, thereby facilitating the uptake and endosomal escape[10].

In this study we developed Vitamin B6 (VitB6) modified pH sensitive charge reversal nanoparticles for efficient intracellular delivery of Doxorubicin (DOX). Herein, VitB6 was conjugated to stearic acid (Figure 1), and lipid nanoparticles was developed by solvent injection method (DOX-B6-SA-NP). Because of the pKa (5.6) of VitB, it remains neutral at physiological pH however it gets positively charged at acidic pH. This charge reversal property makes this carrier system ideal for systemic administration and at the same time it facilitates drug release at acidic pH and thus DOX-B6-SA-NP showed positive charge and enhanced release of DOX at pH 5.

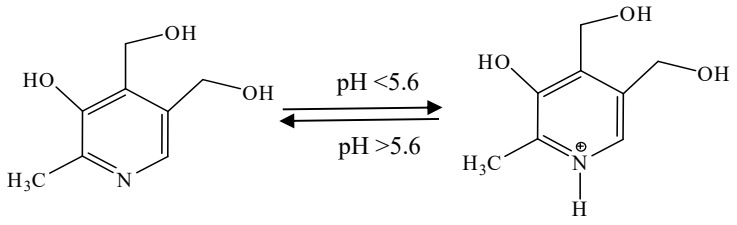

The successful conjugation was confirmed by 1H-NMR. The schematic illustration of NP uptake is shown in Figure 1.

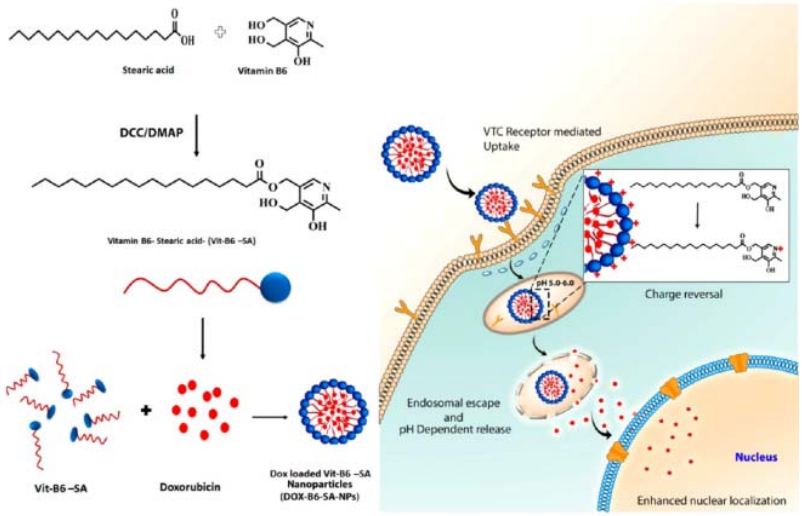

Figure 1: Synthetic Scheme and Schematic Illustration of Intracellular Uptake of Developed NP (DOX-B6-SA-NP) and Triggered Cytoplasmic Release of DOX by Enhanced Endosomal Escape Mediated by pH-Induced Protonation of NPs.

To establish **Endosomal escape** and to determine charge reversal of nanoparticles (DOX-B6-SA-NP) that generate positive charge at acidic conditions of late endosome/lysosome can subsequently disrupt the endosome, a subcellular compartment labeling method was used to observe the distribution of nanoparticles inside the cell (Fig 2). These data confirmed that B6-SA-NP effectively released the FITC in the cells due to their pH responsiveness. Moreover, the B6-SA-NP also facilitated the endosomal escape, which could be due to the proton sponge effect with protonation and regeneration of cationic group lower pH while FITC-SA-NP is non pH sensitive,

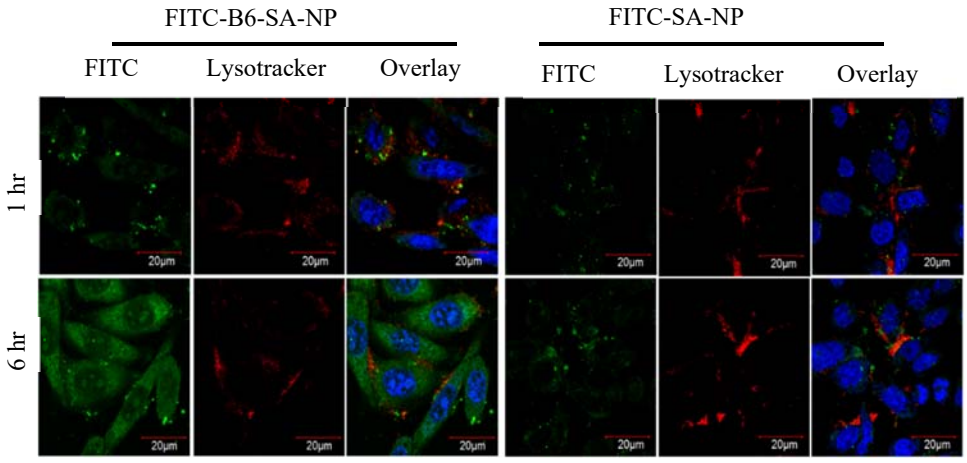

Figure 2: CLSM images of live MDA-MB 231 treated with FITC tagged nanoparticles for 1 hr and 6 hr. Lysotracker (red) was used to stain the acidic organelles of the cell. Scale bar: 20 µ m.

The half inhibitory concentration (IC50) for DOX-B6-SA-NP on MDA-MB 231 cells was 1.76 fold and 3.01 fold lower than free DOX and DOX-SA-NP respectively. The IC50 of DOX-B6-SA-NP on LA 7 cells was found to be 2.01 fold and 4.6 fold lower than free DOX and DOX-SA-NP. The enhanced cell cytotoxicity observed in the cells treated with charge-reversal DOX-B6-SA-NP can be attributed to the improved cell and improved intracellular release (pH triggered). Treatment with DOX-B6-SA-NP for 24 hrs showed around 80% apoptosis including early and late apoptosis, while treatment with free DOX and DOX-SA-NPs resulted in around 45.2% and 19.2% of apoptosis. Thus, the presently described formulation with charge reversing behavior containing DOX induces apoptosis by enhancing the populations of cells arrested in the G2/M phase (Fig 4A).

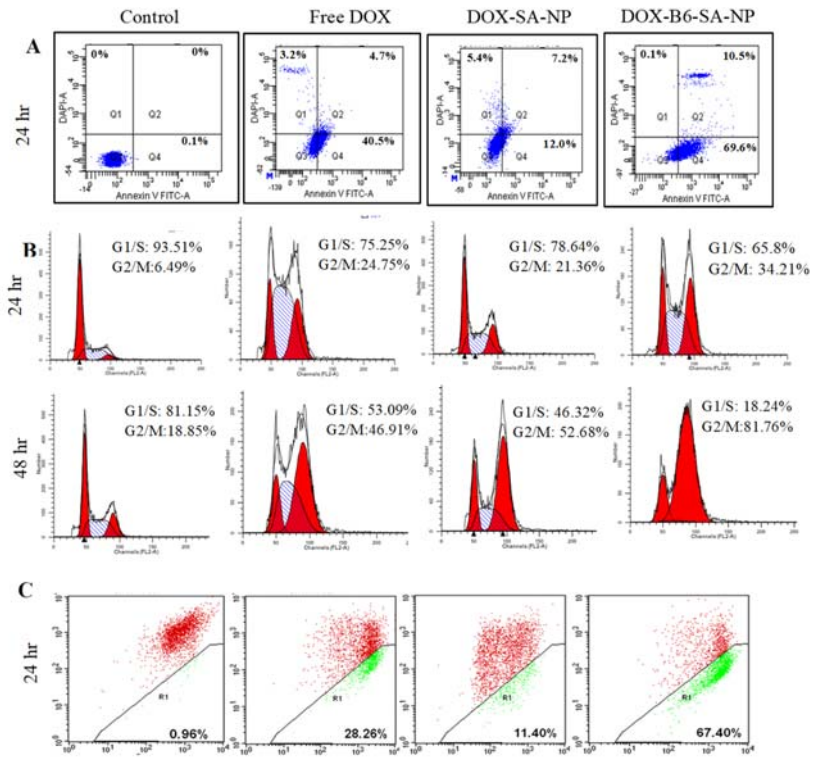

Figure 4: Representative flow cytometry pictures of effect of free DOX and DOX loaded nanoparticles on (A) Apoptosis; (B) Cell cycle; (C) Mitochondrial membrane potential, of MDA-MB 231 cells. (In apoptosis assay Q1 represents the cell population which underwent necrosis, Q2 represent the late apoptotic population, Q3 represent early apoptotic whereas Q4 represents the live cells). All the results were repeated three times and are presented as the mean ± SD, n=3.

Serum distribution profile over 24 hr reveals that DOX-B6-SA-NP groups exhibited 11.53-fold and 1.62 fold increased $AUC_{0-\infty}$ compared to free DOX and DOX-SA-NP, respectively. The average half-life ($t_{1/2}$) of DOX-B6-SA-NP was 6.62 and 1.32 times longer as compared to free DOX and DOX-SA-NP, respectively. These results indicate longer residence of drug in body by DOX-B6-SA-NP which may further expected to promote accumulation at tumor site through the EPR effect. The amount of

DOX in tumors after 24 hrs in DOX-B6-SA-NP treated group was 8.5 fold- and 1.7-fold in comparison to free DOX and DOX-SA-NP treated group. The results indicate that pH sensitive charge conversion nanoparticles render higher accumulation of DOX at tumor site that the other treated groups. The final tumor volume at the end of 20 days in rats of DOX-B6-SA-NP treated group was 37.5, 14.64, 7.8 fold lower than control, free DOX and DOX-SA-NP treated group respectively ($p<0.001$) (Figure 5).

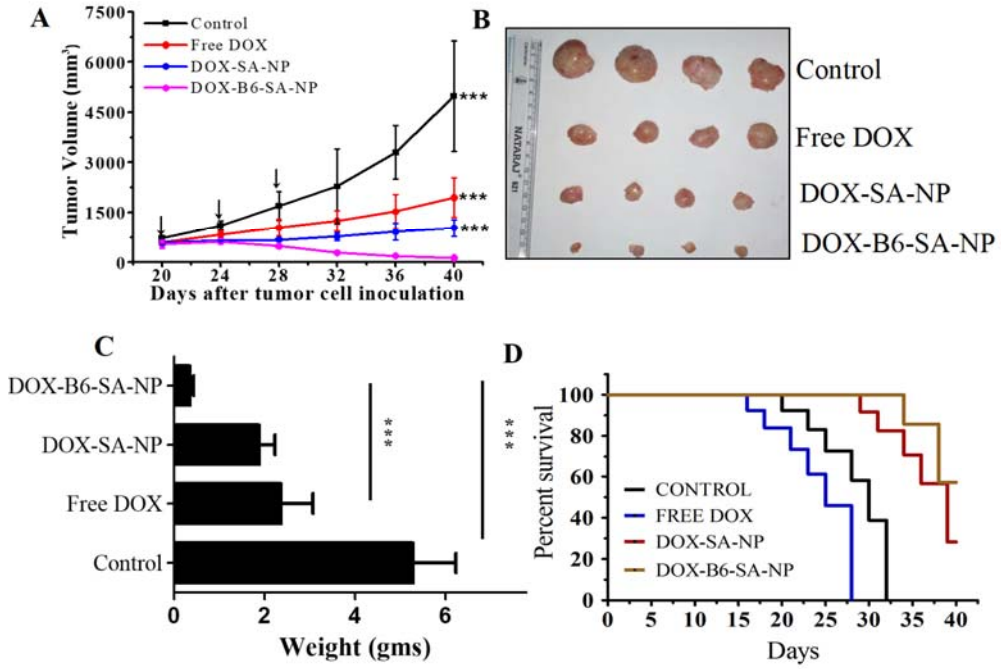

Figure 5: *In-vivo* antitumor activity against LA 7 cells transplanted mammary tumor in SD female rats (DOX dose: 10 mg/ kg body weight): (A) Tumor volume vs time at different time points of the study (n=6); (B) Morphology of the tumors harvested at the end of the study; (C) weights of the tumors excised at the end of the tumor regression study; (D) Survival rates of LA 7 tumor bearing rat administrated with free DOX and DOX loaded nanoparticles (n=6). The x-axis in survival curve represent the number of days after treatment started. (*** = $p<0.001$vs DOX-B6-SA-NP).

ACS APPLIED MATERIALS & INTERFACES
Research Article
www.acsami.org

Vitamin B6 Tethered Endosomal pH Responsive Lipid Nanoparticles for Triggered Intracellular Release of Doxorubicin

Shweta Sharma,[†,§] Ashwni Verma,[†] Jyotsana Singh,[‡,§] B. Venkatesh Teja,[†] Naresh Mittapelly,[†,§] Gitu Pandey,[†,§] Sandeep Urandur,[†] Ravi P. Shukla,[†] Rituraj Konwar,[‡] and Prabhat Ranjan Mishra*[,†,§]

[†]Division of Pharmaceuticsand [‡]Division of Endocrinology, CSIR-Central Drug Research Institute, Lucknow 226031, India
[§]Academy of Scientific and Innovative Research, New Delhi, Delhi 110020, India

8(44), 30407–30421 (2016) ***(Corresponding author)*** ***(I.F. 10.38)***

(ii) we have also established that spermine (SPM) tethered lipo-polymeric hybrid nano-constructs (SPM-D + G/NPs) bearing Doxorubicin and Genistein, interact with cell surface heparan sulfate proteoglycan (HSPG) receptor through receptor-mediated endocytosis and resulted in higher intracellular localization while pH dependent charge reversal in the tumor microenvironment (below pH 5.8) facilitate doxorubicin and Genistein release in a synergistic combination[11,12]. The tumor regression studies confirm that the treatment with prototype nano-constructs led to a significant decrease in tumor growth, and angiogenesis by directing the Akt/Hif1α/VEGF axis as compared to free Dox and Gen alone and their combination. Interestingly, *in silico* docking data indicates direct binding of Doxorubicin and Genistein to key proteins (Akt, Hif1α and VEGFR2) leading to a significant decrease in mRNA and protein levels of Akt, ERK, Hif1α, VEGF-A, VEGFR2, MMP-2 and MMP-9 in human breast cancer cell lines (MDA-MB231) and a xenograft mouse model system. This clearly demonstrates that the developed nano-constructs play a key role in effective management of human breast adenocarcinoma by decreasing the key protein levels involved in apoptosis and angiogenesis processes.

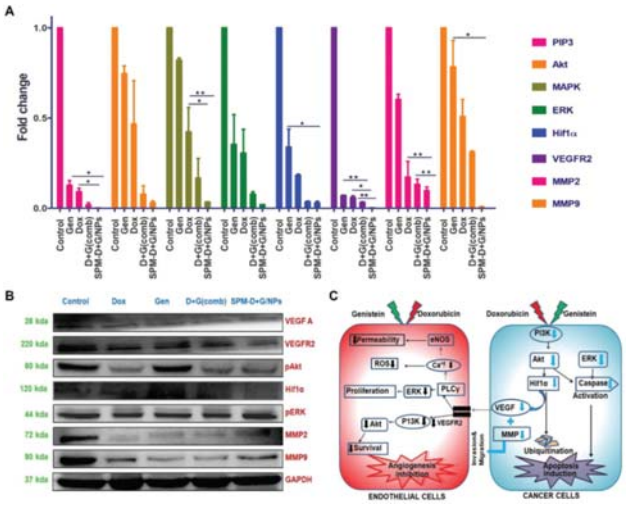

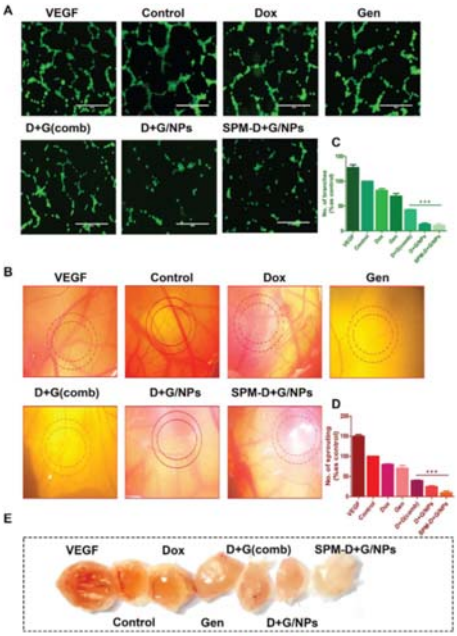

Biomaterials Science

PAPER

Check for updates

Cite this: *Biomater. Sci.*, 2020, **8**, 1298

Multifunctional hybrid nanoconstructs facilitate intracellular localization of doxorubicin and genistein to enhance apoptotic and anti-angiogenic efficacy in breast adenocarcinoma†

Ravi Prakash Shukla,[a] Jayant Dewangan,[b] Sandeep Urandur,[a] Venkatesh Teja Banala,[a] Monika Diwedi,[a] Shweta Sharma,[a] Sristi Agrawal,[a] Srikanta Kumar Rath,[b] Ritu Trivedi[c] and Prabhat Ranjan Mishra[*a]

(iii) We discovered that novel polymeric conjugate comprising chondroitin sulfate A and polyethylene glycol glycol-conjugate possess the propensity to provide stability to , docetaxel (DTX@CSA-NCs) along with stealth effects, and tumor targeting via CD44 receptors, all in one, by developing as a nanocrystalline system of docetaxel with size < 200 nm with pretty higher drug loading ~ 98%. Taking advantage of the enhanced permeability and retention effect coupled with receptor-mediated endocytosis, we established that DTX@CSA-NCs cross the peripheral tumor barrier and penetrate deeper into the cells of the tumor mass. In MDA-MB-231 cells, this enhanced cellular uptake was observed to exhibit a higher degree of cytotoxicity and arrest in the G2 phase in a time dependent fashion. Acting via a mitochondrial-lysosomotropic pathway, DTX@CSA-NCs disrupted the membrane potential and integrity and outperformed the clinically used formulation. Upon intravenous administration, the DTX@CSA-NCs showed better pharmacokinetic profile and excellent 4T1-induced tumor inhibition with significantly less off target toxicity. Thus, this glycoconjugate stabilized nanocrystalline formulation has the potential to take nano-oncology a step forward.

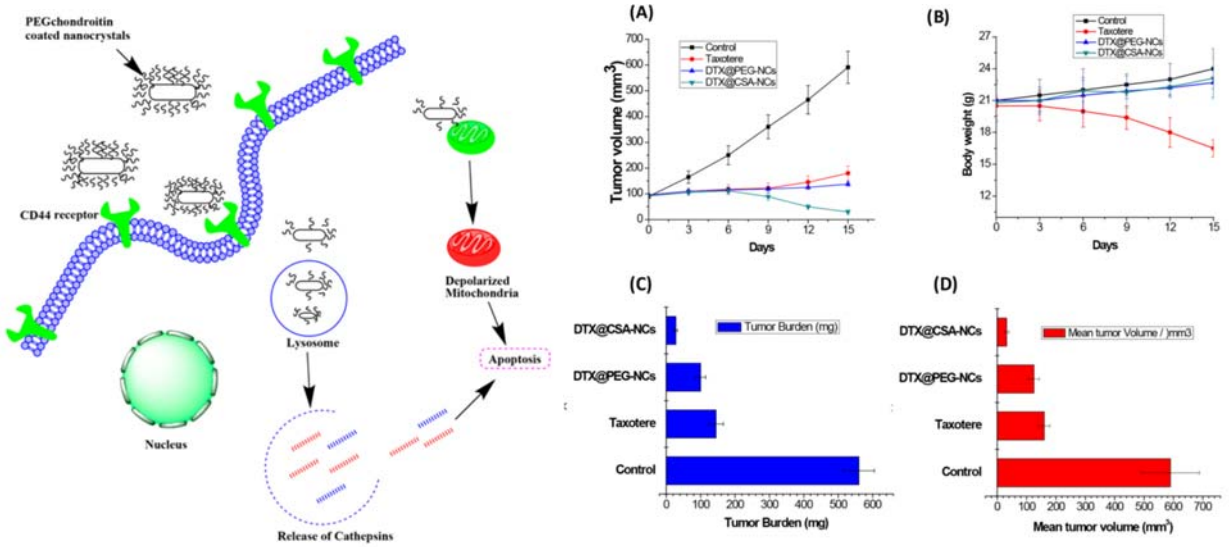

ACS APPLIED MATERIALS & INTERFACES

Research Article

Cite This: ACS Appl. Mater. Interfaces 2018, 10, 16964−16976

www.acsami.org

Multifunctional Glycoconjugate Assisted Nanocrystalline Drug Delivery for Tumor Targeting and Permeabilization of Lysosomal-Mitochondrial Membrane

Gitu Pandey,[†,‡] Naresh Mittapelly,[†,‡] Venkatesh Teja Banala,[†] and Prabhat Ranjan Mishra[*,†,‡]

[†]Pharmaceutics and Pharmacokinetics Division, CSIR−Central Drug Research Institute, Sector 10, Jankipuram Extension, Sitapur Road, Lucknow 226031, Uttar Pradesh, India

[‡]Academy of Scientific and Innovative Research (AcSIR), Training and Development Complex CSIR Campus, CSIR Road, Taramani, Chennai − 600 113, India

10, 16976-16976 2018 (Corresponding author) (I.F. 10.38)

References

(1) Gao, X.; Cui, Y.; Levenson, R. M.; Chung, L. W. K.; Nie, S. Nat. Biotechnol. 2004, 22, 969.
(2) Zhu, Z.; Song, B.; Yuan, J.; Yang, C. Adv. Sci. 2016, 3, No. 1600146.
(3) R.A. Gatenby , R.J. Gillies , Nat. Rev. Cancer 4 (11) (2004) 891.
(4) L. D. Mayer, T. O. Harasym, P. G. Tardi, N. L. Harasym,C. R. Shew, S. A. Johnstone, E. C. Ramsay, M. B. Bally, A. S. Janoff, *Mol. Cancer Ther.* **2006**, *5*, 1854;
(5) R. X. Zhang, P. Cai, T. Zhang, K. Chen, J. Li, J. Cheng, K. S. Pang, H. A. Adissu, A. M. Rauth, X. Y. Wu, *Nanomedicine* **2016**, *12*, 1279.
(6) B. Zhang, T. Wang, S. Yang, Y. Xiao, Y. Song, N. Zhang, S. Garg, *J. Controlled Release* **2016**, *238*, 10.
(7) H. Zhang, D. R. Dunphy, X. Jiang, H. Meng, B. Sun, D. Tarn, M. Xue, X. Wang, S. Lin, Z. Ji, R. Li, F. L. Garcia, J. Yang, M. L. Kirk, T. Xia, J. I. Zink, A. Nel, C. J. Brinker, *J. Am. Chem. Soc.* **2012**, *134*, 15790
(8) Du, J.-Z.; Du, X.-J.; Mao, C.-Q.; Wang, J. J. Am. Chem. Soc. 2011, 133 (44), 17560−17563.
(9) Yezhelyev, M. V.; Qi, L.; O'Regan, R. M.; Nie, S.; Gao, X. J. Am. Chem. Soc. 2008, 130 (28), 9006−9012.
(10) Sahay, G.; Alakhova, D. Y.; Kabanov, A. V. Endocytosis of Nanomedicines. J. Controlled Release 2010, 145 (3), 182−195.
(11) Perry, S. W.; Norman, J. P.; Barbieri, J.; Brown, E. B.; Gelbard, H. A. Mitochondrial membrane potential probes and the proton gradient: a practical usage guide. Biotechniques 2011, 50 (2), 98.
(12) Wen, S.; Zhu, D.; Huang, P. Targeting cancer cell mitochondria as a therapeutic approach. Future medicinal chemistry 2013, 5 (1), 53-67.

[B]TRANSLATIONAL CONTRIBUTION AND COMMERCIALIZATION

We have successfully developed layer-by-layer (LBL) and SMEDDS technology that impacted product development in the area of bone-related disorders. We have been instrumental in patenting 25 technologies, out of which FIVE have been licensed to Industries while TWO are commercialized as Joint FreshTM and ReunionTM [(Granted US patent 8,496,964; AU Patent; 2010217238A; EP patent 2400957 B1) Other products for the treatment of osteoarthritis and bone loss are also developed (Granted US Patent 10,596,115; AU Patent 2014291615; US patent 10265297)]. In addition, he has been actively involved in developing Umifenovir and its formulation under repurposing for COVID patients whose Phase III clinical trial has been completed.

Technologies Commercialized - 02 (TWO)

(i) Development of Nanoemulsion pre-concentrate comprising Standardized Extract of *Spinacea oleracea* (bearing two potential biomarkers K007 and K008) for Improved Efficacy in Osteoarthritis

As a part of **translational research,** a licensed anti-osteoarthritic product based on **nanoemulsion pre-concentrate** comprising standardized extract of *Spinacea oleracea*, has been **launched in the market** and is available as **Joint Fresh™** being marketed by **AERAN Labs.** This formulation contains standardized extract with two identified potential biomarkers that has shown remarkable efficacy *in-vitro* but are not bioavailable *in-vivo* after oral administration. Therefore a SMEDDS based formulation was developed that enhanced the bioavailability of biomarkers and dose was reduced to 150 mg/kg from 750 mg/kg. This strategy was patented and finally licensed to Industry and is now commercialized. This is an important step in bringing the benefits to the public at large by developing a product for **osteoarthritis.**

(ii) Reunion™ Tablets containing standardized extract of *Dalbergia Sissoo* for rapid fracture healing

Another Product **Reunion™** available in the market for rapid fracture healing containing standadrdized extract of *Dalbergia Sissoo* (being marketed by Aeran Labs Pvt. Ltd. This standardized extract contains an active biomarker K024 (Caviunin 7-O-[b-Dapiofuranosyl-(1-6)-b-D-glucopyranoside). As a team member, contributed in estimating K024 biomarker in the tablets and its content uniformity. In addition, has been made to determine and establish the concentration of K024 biomarker in the blood samples of patients and to correlate the biomarker concentration vis-à-vis its efficacy.